1 # Assessment of strict autumn-winter emission controls on air
2 # quality in the Beijing-Tianjin-Hebei region

3 Gongda Lu[1], Eloise A. Marais[2], Tuan V. Vu[1,a], Jingsha Xu[1,b], Zongbo Shi[1], James D. Lee[3,4],
4 Qiang Zhang[5], Lu Shen[6], Gan Luo[7], and Fangqun Yu[7]

5 [1]School of Geography, Earth and Environmental Sciences, University of Birmingham, Birmingham, B15 2TT,
6 UK

7 [2]Department of Geography, University College London, London, WC1E 6BT, UK

8 [3]Wolfson Atmospheric Chemistry Laboratories, University of York, York, YO10 5DD, UK

9 [4]National Centre for Atmospheric Science, University of York, Heslington, York, YO10 5DD, UK

10 [5]Ministry of Education Key Laboratory for Earth System Modeling, Department of Earth System Science,
11 Tsinghua University, Beijing, 100084, China

12 [6]John A. Paulson School of Engineering and Applied Sciences, Harvard University, Cambridge, MA 02138, USA

13 [7]Atmospheric Sciences Research Center, State University of New York at Albany, 251 Fuller Road, Albany, New
14 York, 12203, USA

15 [a]Now at: School of Public Health, Imperial College London, London, W2 1PG, UK

16 [b]Now at: Department of Chemistry, University of Warwick, Coventry, CV4 7AL, UK

17 *Correspondence to*: Gongda Lu (gxl642@student.bham.ac.uk) and Eloise A. Marais (e.marais@ucl.ac.uk)

18 **Abstract.** Strict seasonal emission controls are a popular measure in China for addressing severe air pollution, in

19 particular fine particulate matter ($PM_{2.5}$). Here we evaluate the efficacy of these measures, with a particular focus

20 on the strict emission controls imposed on pollution sources in 28 cities in and around the Beijing-Tianjin-Hebei

21 region (BTH) in autumn-winter 2017/2018. For this we use the GEOS-Chem chemical transport model and air

22 pollutant measurements from the national and Beijing local monitoring networks, after evaluating the network

23 data with independent measurements and correcting large biases in the bottom-up emissions inventory. The

24 network measurements are temporally consistent ($r > 0.9$ for $PM_{2.5}$ and $r > 0.7$ for gases) with the independent

25 measurements, though with systematic differences of 5-17% for nitrogen dioxide (NO_2) and 16-28% for carbon

26 monoxide (CO). The average decrease in monitoring network $PM_{2.5}$ in BTH in autumn-winter 2017/2018 relative

27 to the previous year is 27%, declining from 103 to 75 µg m^{-3}. The regional decline in $PM_{2.5}$ in the model is 20%,

28 exceeding the regional target of 15%. According to the model, pollution control measures led to decline in $PM_{2.5}$

29 precursor emissions of 0.27 Tg NO_x (as NO), 0.66 Tg sulfur dioxide (SO_2), 70 Gg organic carbon (OC), and 50

30 Gg black carbon (BC). We find though that these alone only lead to an 8% decline in $PM_{2.5}$ and that interannual

31 variability in meteorology accounts for more than half (57%) the decline. This demonstrates that year-on-year

32 comparisons are misleading for assessing the efficacy of air pollution measures and should be taken into

33 consideration when extending such measures beyond BTH.

34 ## 1 Introduction

35 Strict seasonal emission controls are an increasingly popular measure to reduce severe air pollution in China, in

36 particular elevated concentrations of fine particles, or $PM_{2.5}$, in autumn-winter. The Chinese government improved

37 such measures in 28 cities in and around the Beijing-Tianjin-Hebei region (BTH) (so-called "2+26" cities) in

38   northern China in autumn and winter 2017/2018. Targets were set to reduce regional mean $PM_{2.5}$ by 15% and

39   city-specific $PM_{2.5}$ by 10-25% relative to the previous year (MEE, 2017). BTH experiences severe air pollution

40   in China despite substantial decline in $PM_{2.5}$ of ~40% from 2013 to 2017 from enacting emission controls as part

41   of the 5-year Action Plans (Zhang et al., 2019). Annual mean $PM_{2.5}$ in BTH in 2017 was 64 µg m^{-3} (Wang et al.,

42   2019); far greater than the national standard of 35 µg m^{-3} (MEE, 2012) and the World Health Organization (WHO)

43   guideline of 10 µg m^{-3}. Severe pollution days (defined as days with 24-hour mean $PM_{2.5} \geq 150$ µg m^{-3}), mostly in

44   autumn and winter, have declined in frequency, but still occurred in 78 days in 2016. Down from 122 days in

45   2013 (Li et al., 2019a). Severe $PM_{2.5}$ pollution is due to a combination of large primary emissions of particles and

46   gas-phase precursors from multiple sources (Zhang et al., 2018), very active heterogeneous chemistry enhancing

47   formation of secondary inorganic and organic aerosols (Huang et al., 2014), and accumulation of pollution due to

48   meteorological conditions such as low windspeeds, shallow planetary boundary layer and high relative humidity

49   (RH) (An et al., 2019; Bei et al., 2020; Le et al., 2020; Wu et al., 2019).

50

51   Dominant local $PM_{2.5}$ sources in BTH in autumn-winter include sustained contributions from the energy sector

52   and road traffic (Tong et al., 2020), and seasonal contributions from industrial and residential combustion of coal

53   and other solid fuels (Ma et al., 2017; Yun et al., 2020), and widespread burning of crop residue (Li et al., 2020c).

54   Mitigation measures in China have led to a nation-wide decrease in emissions of the primary $PM_{2.5}$ components

55   black carbon (BC) and organic carbon (OC) of 28 % for BC and 32 % for OC from 2013 to 2017 (Zheng et al.,

56   2018). Emissions of prominent gas-phase $PM_{2.5}$ precursors such as nitrogen oxides ($NO_x \equiv NO + NO_2$) and sulfur

57   dioxide (SO_2) have declined by 21% for NO_x and 59% for SO_2 over the same time period. Trends in other $PM_{2.5}$

58   precursors are less certain. Emissions of ammonia (NH_3), mostly from agriculture, are likely to have increased or

59   remained constant (Zheng et al., 2018). Similar to NH_3, emissions of non-methane volatile organic compounds

60   (NMVOCs), mostly from industrial activity and solvent use, are either stable or increasing (Li et al., 2019c; Liu

61   et al., 2018b; Zhang et al., 2017a; Zheng et al., 2018). Non-local sources also make a substantial contribution to

62    $PM_{2.5}$ in BTH throughout the year. Dong et al. (2020) used a regional air quality model to estimate that regional

63   transport of non-local $PM_{2.5}$ accounted for 33-68% of total monthly mean $PM_{2.5}$ in BTH in 2017.

64

65   Many mitigation measures were implemented in autumn-winter 2017/2018 to reduce $PM_{2.5}$ in the 28 cities in and

66   around BTH. These are detailed in the "Air Pollution Action Plan in Autumn and Winter of 2017-2018 for the

67   Beijing-Tianjin-Hebei Region and its Surrounding Areas" report by the Chinese Ministry of Ecology and

68   Environment (MEE) (MEE, 2017). Briefly, these include a sector-wide cap on total consumption of coal, phase-

69   out of small inefficient and outdated industrial coal-fired boilers, reduction in production capacity of heavy

70   industries such as iron and cement, switching from coal to cleaner fuels in homes, and mandated controls on

71   construction site fugitive dust emissions. Other short-term and reactionary measures included shutdown of

72   intensive industries and construction sites throughout the emission control period and instantaneous shutdown of

73   additional industrial plants in response to forecasts of elevated $PM_{2.5}$. Tougher emission standards and higher

74   quality vehicular fuel were imposed on on-road vehicles. Agricultural residue burning was banned and strictly

75   enforced, and installation of emission control technologies were mandated for all large emitters of industrial

76   NMVOCs. The MEE used national network observations of $PM_{2.5}$ to determine that regional reduction targets

77   were achieved in BTH and that only 3 of the 28 cities did not meet their city-specific targets (MEE, 2018).

78

79   As demonstrated by studies assessing changes in air quality during the lockdown period in response to the SARS-

80 CoV-2 pandemic, variability in meteorology is also a large contributor to fluctuations in air quality in BTH (Le et

81 al., 2020; Shi et al., 2021). This necessitates that assessment of the efficacy of such measures includes detailed

82 understanding of the contribution of strict emission controls and other factors like meteorology. A recent study

83 by Zhang et al. (2021) assessed city-scale changes in air quality in each of the 28 cities using the high-resolution

84 Community Multi-Scale Air Quality model coupled to the Weather Research and Forecasting Model for

85 meteorology (CMAQ-WRF). CMAQ-WRF was driven with a national bottom-up inventory for the year preceding

86 the emission controls and a regional bottom-up emission inventory for the year of the emission control period.

87 They determined that the contribution of emission controls to the decrease in simulated $PM_{2.5}$ in each city ranged

88 from 2% to 82% and that meteorology was often a dominant contributor, ranging from 18% to 98%. Here we take

89 a regional perspective, after correcting for large biases in the bottom-up emission inventories for BTH with the

90 China national and Beijing regional monitoring network observations which we also assess against independent

91 measurements. We apply the corrected inventory to the GEOS-Chem chemical transport model (CTM) to

92 determine regional-scale emission reductions resulting from strict mitigation measures in autumn-winter

93 2017/2018 and the contribution of these and meteorology to improved regional air quality, as such measures are

94 now widely adopted in China.

95 **2 Air pollutant concentration changes detected with the national and local monitoring networks**

96   Ambient monitoring of $PM_{2.5}$ and trace gases in BTH includes reference monitors from the China National

97 Environmental Monitoring Network (CNEMN) and the local Beijing Municipal Environmental Monitoring

98 Network (BJMEMN) (Zhang et al., 2020). We use observations of hourly SO_2, NO_2, CO, and $PM_{2.5}$ for the

99 autumn-winter emission reduction period (2017/2018) and the preceding year (2016/2017) at sites operational in

100 both years: 402 for CNEMN and 35 for BJMEMN. Data from both networks are from the Sina Air Quality Data

101 Platform (http://beijingair.sinaapp.com/; last accessed 17 October 2020, now hosted at https://quotsoft.net/air/).

102 Data from both networks have been extensively used to quantify changes in surface air pollution (Li et al., 2019b;

103 Silver et al., 2018; Wan et al., 2021; Wang et al., 2014; Zhai et al., 2019), though independent evaluation of the

104 measurements is limited. A previous study used statistical techniques and intercomparison of air pollutant

105 measurements to determine that outliers make only a small contribution ($\leq 1\%$) to measurements of air pollutants

106 relevant to this work (Wu et al., 2018).

107

108   We assess CNEMN and BJMEMN measurements against $PM_{2.5}$ from the US Embassy in Beijing and $PM_{2.5}$ and

109 trace gas (SO_2, NO_2, and CO) measurements from the winter portion of the intensive Atmospheric Pollution &

110 Human Health in a Chinese Megacity (APHH) campaign, hereafter referred to as APHH. The APHH campaign

111 included a comprehensive suite of aerosol and gas-phase measurements from the 325-m tower at the urban

112 Institute of Atmospheric Physics (IAP) measurement site and a few air quality measurements at a rural site (Pinggu)

113 located ~60 km from the Beijing city centre (Shi et al., 2019). APHH data are from the National Environmental

114 Research Council (NERC) Centre for Environmental Data Archive (CEDA) (Fleming et al., 2017). US Embassy

115 $PM_{2.5}$ measurements in Beijing, obtained with US EPA measurement and quality control protocols (Martini et al.,

116 2015), are from the US Department of State Air Quality Monitoring Program (http://www.stateair.net/; last

117 accessed 17 October 2020) for autumn-winter 2016/2017 and from the OpenAQ data portal
118 (http://www.openaq.org/; last accessed 17 October 2020) for autumn-winter 2017/2018. We use APHH data for
119 November-December 2016 and US Embassy $PM_{2.5}$ for October 2016-March 2017 and October 2017-March 2018.
120 These are compared to the nearest national and local monitoring network sites. For APHH, these are the CNEMN
121 Aotizhongxin site (39.98°N, 116.40°E) and the BJMEMN Xizhimenbei site (39.95°N, 116.35°E), each located
122 ~3 km from the APHH urban site (39.97°N 116.37°E). For the US Embassy, these are the CNEMN site
123 Nongzhanguan (39.94°N, 116.46°E) and the BJMEMN site Dongsihuan (39.94°N, 116.48°E), each ~1 km from
124 the US Embassy (39.95°N, 116.47°E).

125

126 Figure 1 compares hourly CNEMN and BJMEMN $PM_{2.5}$ to APHH and US Embassy $PM_{2.5}$. $PM_{2.5}$ from both
127 CNEMN and BJMEMN are temporally consistent with APHH and US Embassy $PM_{2.5}$ ($r \geq 0.96$). The surface
128 monitoring networks also reproduce the variance in hourly $PM_{2.5}$ (Slopes of 1.0-1.1). Network sites are
129 systematically higher than APHH by 10% for CNEMN and 17% for BJMEMN, though compared to US Embassy
130 site $PM_{2.5}$ the difference is small, ranging from negligible (0.2% less) to 6.4% more than US Embassy $PM_{2.5}$. In
131 general, the BJMEMN measurements are 6-17% more than APHH, likely due to spatial variability in local
132 emissions. The decline in $PM_{2.5}$ in the control period relative to the previous year at these sites is 43% according
133 to US Embassy $PM_{2.5}$, decreasing from 97 µg m^{-3} to 55 µg m^{-3}. A similar decline is obtained with the nearby
134 BJMEMN (43% decline) and CNEMN (42% decline) sites shown in Fig. 1.

135

136 Figure 2 compares hourly trace gas measurements from CNEMN, BJMEMN and APHH. The CNEMN and
137 BJMEMN trace gas instruments include chemiluminescence for NO_2, UV fluorescence for SO_2, and IR absorption
138 for CO. Though CO is not a precursor of $PM_{2.5}$, its abundance affects the oxidative potential of the atmosphere
139 and also offers a means to indirectly assess $PM_{2.5}$ precursor emissions of NMVOCs that oxidize to form CO. Most
140 measurements from the local and national networks, with the exception of 31% of the CNEMN SO_2 data and 16%
141 of the BJMEMN SO_2 data, are above the instrument detection limit (indicated in Fig. 2). The surface network is
142 temporally consistent with APHH ($r > 0.7$ for all species). CNEMN NO_2 is <10% more than NO_2 from APHH,
143 likely due to susceptibility of the monitoring network instruments to interference from decomposition of NO_x
144 reservoir compounds to NO_2 (Dunlea et al., 2007; Reed et al., 2016). Shah et al. (2020) estimate a positive bias of
145 ~6% due to this interference. Differences in CNEMN SO_2 (19% less than APHH) and CO (16% more than APHH)
146 are large and reflect differences in variance (CNEMN vs APHH SO_2 slope of 0.8, CNEMN vs APHH CO slope
147 of 1.4). BJMEMN exceeds APHH by 17-28% for all trace gases.

148

149 To aid interpretation of the differences between the network sites and independent measurements, we also assess
150 consistency between CNEMN and BJEMN for the sites shown in Figs. 1 and 2. These are ~5 km apart and the
151 BJEMN site is closer to a heavily trafficked ring road than the CNEMN site. The sites are strongly correlated for
152 $PM_{2.5}$ ($r = 0.97$) and all trace gases ($r = 0.89-0.92$), but CNEMN is less than BJEMN by 11% for NO_2, 33% for
153 SO_2, 9% for CO, and 6% for $PM_{2.5}$ due to the lower relative influence of road traffic sources. This is consistent
154 with the relatively large positive differences between BJEMN and the independent measurements in Figs. 1 and
155 2.

156

157 Both networks also measure ozone, but we do not consider this here, as ozone pollution is most severe in spring
158 and summer in China (Yang et al., 2020). We estimate mean ozone of 15-19 µg m^{-3} at the two monitoring network
159 sites used in Fig. 2. This can be compared to the summer mean ozone air quality metric, mean maximum daily 8-
160 h average ozone, of 120-160 µg m^{-3} in northern China (Li et al., 2019b).

161

162 We show in Fig. 3 the spatial distribution of the network observed changes in air pollutant concentrations in and
163 around BTH in the control period (autumn-winter 2017/2018) relative to the preceding year (autumn-winter
164 2016/2017). In what follows, we refer to these time periods as AW2017 for autumn-winter 2017/2018 and
165 AW2016 for autumn-winter 2016/2017. Only CNEMN and BJMEMN sites that are operational in both periods
166 are used. These include 164 sites within the control domain (region shaded grey in Fig. 3) and 273 sites in the
167 surrounding area. The decline in air pollutant concentrations in AW2017 relative to AW2016 at sites within the
168 emission control region is 16% for NO$_2$, 44% for SO$_2$, 31% for CO, and 29% for PM$_{2.5}$, surpassing the 15% PM$_{2.5}$
169 reduction target set for BTH. Surface concentrations of ozone (not shown) increase by 19% in response to decline
170 in NO$_x$. Even with this increase, ozone is still substantially lower than in spring and summer (Liu et al., 2018a).
171 Smaller reductions of 0.5% for NO$_2$, 31% for SO$_2$, 13% for CO, and 10% for PM$_{2.5}$ occur in the surrounding area.
172 In the southeast portion of the domain shown in Fig. 3, both NO$_2$ and PM$_{2.5}$ increase by 5-8%. Fang et al. (2019)
173 reported an increase in emissions from industries in the non-control area that in Fig. 3 appear to offset air quality
174 improvements that would be expected from decline in influence of pollution from BTH.

175 **3 BTH air pollution and emissions for the year preceding emission controls**

176 We use the GEOS-Chem model (version 12.0.0; https://doi.org/10.5281/zenodo.1343547) with the evaluated
177 surface network measurements to constrain precursor emissions of PM$_{2.5}$ in and around BTH. The model is nested
178 over East Asia (11°S-55°N, 60-150°E) at a horizontal resolution of 0.5° × 0.625° (latitude × longitude). The model
179 is driven with assimilated meteorology from the NASA Modern-Era Retrospective analysis for Research and
180 Applications version 2 (MERRA-2) updated hourly for 2D fields and every 3 hours for 3D fields. Dynamic (3-
181 hourly) boundary conditions are from a global simulation at 4° × 5°. Monthly anthropogenic emissions for China
182 in AW2016 are from the regional bottom-up Multi-resolution Emission Inventory for China (MEIC)
183 (http://www.meicmodel.org/; last accessed 4 March 2020) available for 2000-2017 at 0.5° × 0.625°. MEIC
184 includes emissions of SO$_2$, NO$_x$, CO, NMVOCs, NH$_3$, and primary particles from ~700 anthropogenic sources
185 (Zheng et al., 2018; Li et al., 2017). In its implementation in GEOS-Chem, MEIC emissions are lumped into five
186 sectors: industry, power plants, transportation, agriculture and residential. Primary particles are emitted as
187 hydrophobic and hydrophilic BC and OC, and speciated NMVOCs are mapped to those in GEOS-Chem using the
188 NMVOCs species mapping tables in Li et al. (2014).

189

190 The model includes detailed coupled gas- and aerosol-phase chemistry to represent the formation and loss of PM$_{2.5}$.
191 Individual aerosol components are modelled as externally mixed. These include sulfate, nitrate, ammonium (Park
192 et al., 2004; Wang et al., 2013), OC (Heald et al., 2006), BC (Li et al., 2016), dust (Fairlie et al., 2007), and sea
193 salt (Jaegle et al., 2011). Formation of secondary sulfate-nitrate-ammonium aerosols are computed with
194 ISORROPIA-II (Fountoukis and Nenes, 2007). Physical loss processes include dry and wet deposition (Amos et
195 al., 2012; Liu et al., 2001; Wang et al., 1998). We implement a revised treatment of wet scavenging described and

196   first implemented in GEOS-Chem by Luo et al. (2019). This replaces fixed values of in-cloud condensation water
197   with dynamic values from MERRA-2. This leads to more rapid wet deposition rates and addresses a positive bias
198   in modelled nitrate and ammonium, in particular in winter, when compared to surface observations in China,
199   Europe, and the US (Luo et al., 2020). We sample the model in AW2016 and AW2017 following two months
200   spin-up before each period of interest for chemical initialization.

202   We find from initial comparison of the model to the surface observations that the model in AW2016 is
203   considerably less than observed NO_2 (by 48%), SO_2 (by 42%), and CO (by 57%) over the entire domain shown
204   in Fig. 3. We attribute this to an underestimate in precursor emissions of these in the MEIC. Previous studies
205   reported that MEIC trends in NO_x, SO_2, and CO emissions are consistent with trends in satellite observations of
206   column densities and weather-normalised surface measurements (Vu et al., 2019; Zheng et al., 2018), but studies
207   assessing and identifying similar underestimates to ours are limited to very local assessment of the inventory.
208   Squires et al. (2020) determined that MEIC NO_x and CO emissions are overestimated at the urban APHH site
209   from comparison to fluxes calculated using the eddy-covariance method, though their comparison was for
210   different years (measurements in 2016, MEIC in 2013). We calculate scale factors to apply to the MEIC based on
211   our initial comparison to the network site measurements. These include spatially uniform scale factors of 1.5
212   applied to NO_x emissions and 2.4 applied to CO emissions across the whole domain shown in Fig. 3. Spatially
213   variable scale factors of 2.1-6.8 are applied to seven grid squares for the MEIC SO_2 emissions. These are
214   concentrated in Shanxi province west of BTH, a region with large coal-fired power plants (Xie et al., 2018). These
215   grids account for the majority of the domain average 42% underestimate in modelled SO_2 concentrations. Local
216   enhancements in CO can include primary emissions and secondary contributions from oxidation of NMVOCs.
217   Emission inventory estimates of NMVOCs are subject to large uncertainties, mainly due to poorly quantified
218   industrial emissions (Li et al., 2017) and lack of reliable data for scattered areal sources such as residential coal
219   burning (Li et al., 2019c; Peng et al., 2019; Shi et al., 2020). We find though that modelled CO is relatively
220   unaffected by NMVOCs emissions. A sensitivity simulation with MEIC NMVOCs emissions increased by 50%
221   only increases surface CO concentrations by 0.2%. Given this, we attribute the model underestimate in CO surface
222   concentrations to the emissions. We do not adjust MEIC primary emissions of BC and OC, due to limited
223   constraints on these from the observations. APHH eddy covariance fluxes of BC obtained in winter suggest a
224   large overestimate (59 times) in MEIC BC emissions (Joshi et al., 2021), though this may be due to very local
225   influence of traffic that is diluted at the resolution of the MEIC (Joshi et al., 2021).

227   Figure 4 compares GEOS-Chem and monitoring network air pollutant concentrations for BTH and the
228   surrounding area after applying scale factors to MEIC emissions of SO_2, NO_x, and CO. Emissions scaling of NO_x
229   improves the modelled variance in NO_2. The regression slope increases from 0.86 (not shown) to 0.93 (Fig. 4).
230   There is still an underestimate in modelled background NO_2 (intercept = -12.8 µg m^{-3}) that leads to a model NO_2
231   normalized mean bias (NMB) of -33%. The monitoring network includes sites close to busy roads that may be
232   influenced by local traffic emissions that would be diluted at the 50-67 km resolution of the model. The BJMEMN
233   sites are categorised by location and we find that excluding roadside sites leads to a 5-8% decrease in mean
234   BJMEMN NO_2 (2-8% decrease for the other pollutants) and would only partially resolve the remaining
235   underestimate in modelled NO_2 in Fig. 4. Other factors that could contribute to the remaining discrepancy include

236   short atmospheric lifetime of NO_2, relatively coarse model resolution, and a positive 5-17% bias in the monitoring

237   network measurements (Fig. 2). Any further increases in MEIC NO_x emissions would worsen the model NMB in

238    $PM_{2.5}$ of 15%, as nitrate from oxidation of NO_x is the dominant component of $PM_{2.5}$ (29% in AW2016 for the

239   entire domain in Fig. 3, according to GEOS-Chem).

240

241   Emissions scaling of SO_2 improves spatial consistency for concentrations of SO_2 from $r = 0.54$ (not shown) to r

242    $= 0.90$ (Fig. 4). There is still a model bias -29% mostly due to 2 grids in Shanxi province with observed SO_2 of

243   161-200 µg m^{-3} and modelled SO_2 of 109-122 µg m^{-3} (Fig. 4). The model underestimate in CO decreases from -

244   57% to -14% and the remaining model bias may be due to a 16-28% positive bias in the monitoring network (Fig.

245   2). The improvement in spatial correlation for CO is marginal, increasing from $r = 0.35$ to $r = 0.45$. Scaling MEIC

246   emissions of SO_2 and NO_x increases the modelled $PM_{2.5}$ NMB from 8% with the original emissions to 15% with

247   the scaled emissions. This may be due to remaining uncertainties in MEIC emissions of BC, OC, and NH_3.

248

249   Figure 5 compares observed and modelled $PM_{2.5}$ composition at the urban and rural APHH sites. The model

250   overestimates total $PM_{2.5}$ by 10% at the urban site and 34% at the rural site. Components are measured with a

251   semicontinuous analyzer for OC and BC (Han et al., 2014; Kondo et al., 2006) and ion chromatography following

252   particle collection with a Partisol for sulfate, nitrate, and ammonium (Taiwo et al., 2014; Xu et al., 2021). OC is

253   compared instead of organic aerosol (OA), due to uncertainties in conversion of OC to OA (Xing et al., 2013).

254   According to the observations, OC is the dominant $PM_{2.5}$ component, with a carbon mass contribution to total

255    $PM_{2.5}$ of 23% at the urban site and 33% at the rural site. The total contribution of secondary inorganic aerosols is

256   similar (31%) at both sites and includes 9% sulfate, 13% nitrate, and 9% ammonium at the urban site and similar

257   contributions (8% sulfate, 13% nitrate, and 10% ammonium) at the rural site. BC is 4% of total $PM_{2.5}$ at both sites.

258   The model underestimates OC (9% urban, 10% rural) and sulfate (both 4%), overestimates nitrate (28%, 30%),

259   slightly overpredicts BC (4%, 5%), and is similar for ammonium (both 10%).

260

261   Previous studies have reported similar biases in simulated OC, sulfate and nitrate in China from GEOS-Chem

262   (Miao et al., 2020) and other CTMs (Chen et al., 2019; Gao et al., 2018). Miao et al. (2020) reported a year-round

263   underestimate in OA that they attribute to biases in precursor emissions and lack of seasonality in fixed secondary

264   OA (SOA) yields used to estimate SOA formation from precursor emissions of NMVOCs. They also identified a

265   year-round underestimate in sulfate that peaks at 54% in winter (Miao et al., 2020), similar to the 50%

266   underestimate we obtain at the urban IAP site. The model underestimate in sulfate may in part be due to the

267   remaining underestimate in MEIC SO_2 emissions (Fig. 4) after scaling MEIC SO_2 emissions. The model may also

268   be missing key sulfate formation processes during haze events (Bloss et al., 2021; Wang et al., 2016; Wang et al.,

269   2020), though the measurements may also be impacted by interference from hydroxymethane sulfonate (HMS)

270   (Moch et al., 2018; Song et al., 2019). The overestimate in modelled nitrates is a common issue and has been

271   attributed by Miao et al. (2020) to an overestimate in aerosol nitrate precursors at night exacerbated by errors in

272   boundary layer dynamics. Despite biases in $PM_{2.5}$ composition, the model reproduces day-to-day variability in

273   24-hour mean $PM_{2.5}$ ($r = 0.66-0.71$) and its components ($r = 0.50-0.78$) at both sites.

274

275 Figure 6 shows total anthropogenic emissions of gaseous PM$_{2.5}$ precursors and primary PM$_{2.5}$ (OC and BC) for
276 AW2016 obtained after applying scaling factors to the MEIC based on discrepancies in modelled and observed
277 air pollutant concentrations. Total anthropogenic emissions in BTH (area shaded grey in Fig. 3) in AW2016, the
278 year prior to the control period, are 2.4 Tg NO$_x$ as NO, 1.6 Tg SO$_2$, 150 Gg BC, 240 Gg OC, and 41 Tg CO.
279 NMVOCs (2.0 Tg C) and NH$_3$ (0.64 Tg) are not shown in Fig. 6, as these are unchanged from AW2016 to
280 AW2017. Though emissions of NO$_x$, CO and SO$_2$ increase in AW2016 relative to the default MEIC emissions
281 due to our emissions scaling, there is no change in the relative contribution of different sectors. The major sector
282 contributions include industry for NO$_x$ (44%), SO$_2$ (56%), and CO (39%), transport for NO$_x$ (34%), and residential
283 fuel use for domestic heating and cooking for SO$_2$ (28%), CO (42%), BC (47%) and OC (79%).

4 Influence of emissions and meteorology on air quality in AW2017

285 To estimate the emission changes in the model due to controls implemented in BTH in AW2017, we regrid the
286 relative changes in the surface air quality observations (Fig. 3) to a $1° \times 1.25°$ resolution grid to achieve reasonably
287 extensive coverage across the whole domain shown in Fig. 3. For grids without surface observations (17% of the
288 grids in the emission control region, 51% outside it), we interpolate across nearest neighbouring grids.
289 Anthropogenic emissions beyond the geographic limits in Fig. 3 are unchanged. Due to lack of observations of
290 OC and BC concentrations, we initially use the relative change in total measured PM$_{2.5}$. This ranges from a
291 decrease in AW2017 relative to AW2016 of 5% to 53% in BTH. We find with this initial approach that the model
292 underestimates the percent reduction in PM$_{2.5}$ in AW2017 relative to AW2016. This suggests that the decline in
293 primary PM$_{2.5}$ may be greater than the decline in total PM$_{2.5}$, corroborated by the greater decline in primary PM$_{2.5}$
294 emissions in the bottom-up inventories used by Zhang et al. (2021) than the decline in measured total PM$_{2.5}$ for
295 around half of the 28 cities. This may be because the regulations mostly targeted sources that have large primary
296 PM$_{2.5}$ emissions, such as coal combustion, industry, vehicles, fugitive dust and biomass burning (Zhang et al.,
297 2017b; Zheng et al., 2017). We iterate to obtain BC and OC emissions scaling factors that are 1.4 times more than
298 the percent change in total PM$_{2.5}$.

300 Figure 7 shows the spatial distribution of modelled and observed PM$_{2.5}$ concentrations and relative changes in
301 PM$_{2.5}$ in and around BTH. The average decrease in observed PM$_{2.5}$ is 28% in BTH, declining from 103 µg m^{-3} in
302 AW2016 to 75 µg m^{-3} in AW 2017. A similar decline is obtained with the model for grids coincident with the
303 sites (25% decrease from 112 µg m^{-3} in AW2016 to 85 µg m^{-3} in AW2017). The decline in modelled PM$_{2.5}$ for all
304 BTH grids is 20% and compared to 16% for the whole domain. In Beijing, observed PM$_{2.5}$ decreases from 96 µg
305 m^{-3} in AW2016 to 57 µg m^{-3} in AW2017, a 40% reduction. The decline in the model for all 13 grids covering
306 Beijing (39.25-41.25°N, 115.3125-117.8125°E) is more modest (33% decline from 75 µg m^{-3} in AW2016 to 50
307 µg m^{-3} in AW2017) than the grids coincident with the monitoring network sites. Regardless, both values exceed
308 the 25% target set for Beijing (MEE, 2017).

310 Figure 8 further compares observed and modelled relative changes in PM$_{2.5}$. This confirms the skill of the model
311 at reproducing the relative change in PM$_{2.5}$, despite an overall positive bias in total PM$_{2.5}$ (Figs. 4 and 7) and
312 individual PM$_{2.5}$ components (Fig. 5). The modelled relative changes in PM$_{2.5}$ are somewhat more spatially
313 consistent with the observations in BTH ($r = 0.82$) than the surrounding area ($r = 0.76$). The variance is closer to

314   unity for BTH (slope = 0.84) than the surrounding area (slope = 0.74). The relative change in $PM_{2.5}$ outside the

315   emission control domain is -10% according to the observations, and -11% in the coincident model grids. During

316   the emission control period, the area surrounding BTH in the domain shown in Fig. 7 is likely influenced by

317   anthropogenic emissions from neighbouring regions that are the same in AW2017 and AW2016. This may account

318   for the differences in the direction of change for 14 model grids (decline) compared to the observations (increase)

319   in Fig. 8.

320

321   The emissions that we estimate for the control period (AW2017) are also shown in Fig. 6. According to our

322   approach, total emissions reductions in AW2017 compared to AW2016 in BTH are 0.27 Tg NO_x as NO, 0.66 Tg

323   SO_2, 9.7 Tg CO, 70 Gg OC, and 50 Gg BC. Emissions of NH_3 and NMVOCs are unchanged due to limited

324   constraints on these. There is an Ammonia Monitoring Network in China (AMoN-China), but there are only 8

325   sites in BTH, and the data are not publicly available (Pan et al., 2018). Relating NH_3 concentrations to emissions

326   is also complicated by its ability to partition to sulfate aerosols (Fu et al., 2017) that decline by 36%, according to

327   the model, in AW2017 relative to AW2016 due to decline in SO_2 emissions. There were also no mandatory

328   measures targeting NH_3 sources during AW2017. Agricultural activities such as fertilizer and livestock excreta

329   (Huang et al., 2012), dominant NH_3 sources in China, are also at a minimum in autumn and winter (Kong et al.,

330   2019). Zhang et al. (2021) reported that NH_3 emissions were relatively unchanged in almost half of the 28 cities

331   and varied in others from a 35% decrease to a 33% increase. Controls in BTH in AW2017 should have targeted

332   NMVOCs sources, but these have limited effect on $PM_{2.5}$ according to GEOS-Chem. The sensitivity simulation

333   we conducted with a 50% increase in NMVOCs emissions only causes a 1% increase in surface concentrations of

334   $PM_{2.5}$. Mechanisms leading to the formation of wintertime SOA are not well understood. Field campaigns in

335   winter in Beijing suggest significant SOA formation from oxidation of NMVOCs (Li et al., 2020a; Li et al., 2020b),

336   whereas Wang et al. (2021) propose that rapid aqueous-phase oxidation of primary OA dominates SOA formation

337   and would resolve the observed decline in SOA in Beijing in winter at the same time that NMVOCs emissions

338   have remained relatively constant.

339

340   We also quantify the contribution of meteorology to the decline in $PM_{2.5}$ in AW2017. To do this, we compare

341   modelled $PM_{2.5}$ from the AW2017 simulation (Fig. 7) to a simulation with AW2017 emissions and AW2016

342   meteorology. The decline in $PM_{2.5}$ in BTH due to differences in AW2016 and AW2017 meteorology only is 12

343   $\mu g\ m^{-3}$ or 57% of the decline in $PM_{2.5}$ from changes in both emissions and meteorology. The contribution of

344   meteorology is similar, 54%, in the surrounding area. Our estimate is slightly less than the city-scale study by

345   Zhang et al. (2019). They attribute 70% of the decline in $PM_{2.5}$ in BTH to variation in meteorology using CMAQ

346   driven with WRF meteorology and the national MEIC and regional Beijing emissions inventories. Zhang et al.

347   (2021) identified large variability in the contribution of emissions and meteorology to decline in $PM_{2.5}$ across the

348   28 cities, of 2-82% for emissions and 18-98% for meteorology. We find that the meteorological factors

349   contributing to decline in $PM_{2.5}$ in BTH in AW2017 include dilution and dispersion of pollution due to stronger

350   south-easterly winds and a 7% higher planetary boundary layer in AW2017 than AW2016. Efficiency of formation

351   of secondary inorganic aerosols would also be less in AW2017 than AW2016 in response to 5% lower RH.

352   Interannual variability in RH has similarly been identified as the cause for sustained air pollution over BTH despite

353   a dramatic decline in precursor emissions from lockdown measures imposed to mitigate the spread of the SARS-

354 CoV-2 virus (Le et al., 2020). The meteorological factors that we identified with GEOS-Chem are consistent with
355 those identified by Zhang et al. (2021) using WRF.

5 Conclusions

357 Strict emission controls were implemented across 28 cities in and around the Beijing-Tianjin-Hebei region (BTH)
358 in autumn-winter 2017/2018 to address severe air pollution, specifically fine particles ($PM_{2.5}$). We used national
359 and local surface monitoring network observations of $PM_{2.5}$ and trace gases with the GEOS-Chem model to assess
360 the efficacy of emission controls, following evaluation of the network with independent measurements.

362 $PM_{2.5}$ and trace gases (NO_2, SO_2 and CO) from the surface networks are temporally consistent with independent
363 measurements ($r > 0.9$ for $PM_{2.5}$ and $r > 0.7$ for gases) and exhibit discrepancies that are in large part due to
364 variability of these in the urban environment. According to these networks, $PM_{2.5}$ in BTH decreased by 28% from
365 103 µg m^{-3} to 75 µg m^{-3} in the control period relative to the previous year, exceeding the regional target of 15%.
366 The model with emissions scaled to address large biases in NO_x, SO_2, and CO emissions, reproduces the spatial
367 distribution in $PM_{2.5}$ ($r = 0.68$). Despite a 15% positive bias in total $PM_{2.5}$ and large biases in $PM_{2.5}$ composition,
368 the model captures the relative decline in $PM_{2.5}$ in BTH of 25%. According to the model constrained with the
369 network measurements, decline in emissions in BTH due to strict controls are 0.27 Tg NO_x as NO, 0.66 Tg SO_2,
370 9.7 Tg CO, 70 Gg OC, and 50 Gg BC. These account for less than half the observed decline in $PM_{2.5}$ and alone
371 lead to an 8% reduction in $PM_{2.5}$, falling shorting of $PM_{2.5}$ reduction target. The remainder is due to meteorology,
372 specifically a deeper planetary boundary layer, stronger winds, and lower relative humidity during the control
373 period.

375 This supports the need for much stricter emissions controls in BTH and other parts of China where these controls
376 are now adopted.

Data Availability

378 The GEOS-Chem model outputs used in this study are available at:
379 https://github.com/GongdaLu/BTH_emission_control.

Author Contributions

381 GLu performed the GEOS-Chem simulations, analysed the model and measurement data, and prepared the
382 manuscript. EAM assisted in the writing and provided supervisory guidance, with co-supervision and editorial
383 contributions from ZS. JDL provided APHH gas concentration data. ZS, TVV and JX performed PM composition
384 analyses and provided guidance on using APHH data. QZ provided the original MEIC emission inventory that LS
385 processed for input to GEOS-Chem. GLuo and FY provided source codes for the updated wet scavenging scheme
386 in GEOS-Chem.

Competing Interests

388 The authors declare that they have no conflicts of interest.

389 **Acknowledgements**

390 This work was funded by a China Scholarship Council scholarship awarded to GLu and a NERC/EPSRC grant

391 (grant number EP/R513465/1) awarded to EAM. ZS acknowledges funding from the NERC APHH-Beijing

392 programme (grant number NE/N007190/1).

393

394 **References**

395 Amos, H. M., Jacob, D. J., Holmes, C. D., Fisher, J. A., Wang, Q., Yantosca, R. M., Corbitt, E. S., Galarneau, E.,
396 Rutter, A. P., Gustin, M. S., Steffen, A., Schauer, J. J., Graydon, J. A., St Louis, V. L., Talbot, R. W., Edgerton,
397 E. S., Zhang, Y., and Sunderland, E. M.: Gas-particle partitioning of atmospheric Hg(II) and its effect on global
398 mercury deposition, Atmos. Chem. Phys., 12, 591-603, https://doi.org/10.5194/acp-12-591-2012, 2012.

399 An, Z., Huang, R. J., Zhang, R., Tie, X., Li, G., Cao, J., Zhou, W., Shi, Z., Han, Y., Gu, Z., and Ji, Y.: Severe haze
400 in northern China: A synergy of anthropogenic emissions and atmospheric processes, Proc. Natl. Acad. Sci. USA,
401 116, 8657-8666, https://doi.org/10.1073/pnas.1900125116, 2019.

402 Bei, N., Li, X., Tie, X., Zhao, L., Wu, J., Li, X., Liu, L., Shen, Z., and Li, G.: Impact of synoptic patterns and
403 meteorological elements on the wintertime haze in the Beijing-Tianjin-Hebei region, China from 2013 to 2017,
404 Sci. Total. Environ., 704, 135210, https://doi.org/10.1016/j.scitotenv.2019.135210, 2020.

405 Bloss, W. J., Kramer, L., Crilley, L. R., Vu, T., Harrison, R. M., Shi, Z., Lee, J. D., Squires, F. A., Whalley, L.
406 K., Slater, E., Woodward-Massey, R., Ye, C., Heard, D. E., Tong, S., Hou, S., Sun, Y., Xu, J., Wei, L., and Fu,
407 P.: Insights into air pollution chemistry and sulphate formation from nitrous acid (HONO) measurements during
408 haze events in Beijing, Faraday Discuss., 226, 223-238, 10.1039/d0fd00100g, 2021.

409 Chen, L., Gao, Y., Zhang, M. G., Fu, J. S., Zhu, J., Liao, H., Li, J. L., Huang, K., Ge, B. Z., Wang, X. M., Lam,
410 Y. F., Lin, C. Y., Itahashi, S., Nagashima, T., Kajino, M., Yamaji, K., Wang, Z. F., and Kurokawa, J.: MICS-Asia
411 III: multi-model comparison and evaluation of aerosol over East Asia, Atmos. Chem. Phys., 19, 11911-11937,
412 https://doi.org/10.5194/acp-19-11911-2019, 2019.

413 Dong, Z., Wang, S., Xing, J., Chang, X., Ding, D., and Zheng, H.: Regional transport in Beijing-Tianjin-Hebei
414 region and its changes during 2014-2017: The impacts of meteorology and emission reduction, Sci. Total.
415 Environ., 737, 139792, https://doi.org/10.1016/j.scitotenv.2020.139792, 2020.

416 Dunlea, E. J., Herndon, S. C., Nelson, D. D., Volkamer, R. M., San Martini, F., Sheehy, P. M., Zahniser, M. S.,
417 Shorter, J. H., Wormhoudt, J. C., Lamb, B. K., Allwine, E. J., Gaffney, J. S., Marley, N. A., Grutter, M., Marquez,
418 C., Blanco, S., Cardenas, B., Retama, A., Villegas, C. R. R., Kolb, C. E., Molina, L. T., and Molina, M. J.:
419 Evaluation of nitrogen dioxide chemiluminescence monitors in a polluted urban environment, Atmos. Chem.
420 Phys., 7, 2691-2704, https://doi.org/10.5194/acp-7-2691-2007, 2007.

421 Fairlie, T. D., Jacob, D. J., and Park, R. J.: The impact of transpacific transport of mineral dust in the United States,
422 Atmos. Environ., 41, 1251-1266, https://doi.org/10.1016/j.atmosenv.2006.09.048, 2007.

423 Fang, D., Chen, B., Hubacek, K., Ni, R., Chen, L., Feng, K., and Lin, J.: Clean air for some: Unintended spillover
424 effects of regional air pollution policies, Sci. Adv., 5, eaav4707, https://doi.org/10.1126/sciadv.aav4707, 2019.

425 Fleming, Z. L., Lee, J. D., Liu, D., Acton, J., Huang, Z., Wang, X., Hewitt, N., Crilley, L., Kramer, L., Slater, E.,
426 Whalley, L., Ye, C., and Ingham, T.: APHH: Atmospheric measurements and model results for the Atmospheric
427 Pollution & Human Health in a Chinese Megacity, available at:
428 http://catalogue.ceda.ac.uk/uuid/648246d2bdc7460b8159a8f9daee7844 (last access: 04 March 2021), 2017.

429 Fountoukis, C. and Nenes, A.: ISORROPIA II: a computationally efficient thermodynamic equilibrium model for
430 K^+-Ca^{2+}-Mg^{2+}-NH_4^+-Na^+-SO_4^{2-}-NO_3^--Cl^--H_2O aerosols, Atmos. Chem. Phys., 7, 4639-4659,
431 https://doi.org/10.5194/acp-7-4639-2007, 2007.

432 Fu, X., Wang, S. X., Xing, J., Zhang, X. Y., Wang, T., and Hao, J. M.: Increasing Ammonia Concentrations
433 Reduce the Effectiveness of Particle Pollution Control Achieved via SO_2 and NO_X Emissions Reduction in East
434 China, Environ. Sci. Tech. Lett., 4, 221-227, https://doi.org/10.1021/acs.estlett.7b00143, 2017.

435 Gao, M., Han, Z. W., Liu, Z. R., Li, M., Xin, J. Y., Tao, Z. N., Li, J. W., Kang, J. E., Huang, K., Dong, X. Y.,
436 Zhuang, B. L., Li, S., Ge, B. Z., Wu, Q. Z., Cheng, Y. F., Wang, Y. S., Lee, H. J., Kim, C. H., Fu, J. S. S., Wang,
437 T. J., Chin, M. A., Woo, J. H., Zhang, Q., Wang, Z. F., and Carmichael, G. R.: Air quality and climate change,
438 Topic 3 of the Model Inter-Comparison Study for Asia Phase III (MICS-Asia III) - Part 1: Overview and model
439 evaluation, Atmos. Chem. Phys., 18, 4859-4884, https://doi.org/10.5194/acp-18-4859-2018, 2018.

440 Han, T. T., Liu, X. G., Zhang, Y. H., Qu, Y., Gu, J. W., Ma, Q., Lu, K. D., Tian, H. Z., Chen, J., Zeng, L. M., Hu,
441 M., and Zhu, T.: Characteristics of Aerosol Optical Properties and Their Chemical Apportionments during
442 CAREBeijing 2006, Aerosol Air Qual. Res., 14, 1431-1442, https://doi.org/10.4209/aaqr.2013.06.0203, 2014.

443 Heald, C. L., Jacob, D. J., Turquety, S., Hudman, R. C., Weber, R. J., Sullivan, A. P., Peltier, R. E., Atlas, E. L.,
444 de Gouw, J. A., Warneke, C., Holloway, J. S., Neuman, J. A., Flocke, F. M., and Seinfeld, J. H.: Concentrations
445 and sources of organic carbon aerosols in the free troposphere over North America, J. Geophys. Res. Atmos., 111,
446 D23S47, https://doi.org/10.1029/2006jd007705, 2006.

447 Huang, R. J., Zhang, Y., Bozzetti, C., Ho, K. F., Cao, J. J., Han, Y., Daellenbach, K. R., Slowik, J. G., Platt, S.
448 M., Canonaco, F., Zotter, P., Wolf, R., Pieber, S. M., Bruns, E. A., Crippa, M., Ciarelli, G., Piazzalunga, A.,
449 Schwikowski, M., Abbaszade, G., Schnelle-Kreis, J., Zimmermann, R., An, Z., Szidat, S., Baltensperger, U., El
450 Haddad, I., and Prevot, A. S.: High secondary aerosol contribution to particulate pollution during haze events in
451 China, Nature, 514, 218-222, https://doi.org/10.1038/nature13774, 2014.

452 Huang, X., Song, Y., Li, M. M., Li, J. F., Huo, Q., Cai, X. H., Zhu, T., Hu, M., and Zhang, H. S.: A high-resolution
453 ammonia emission inventory in China, Global Biogeochem. Cy., 26, GB1030,
454 https://doi.org/10.1029/2011gb004161, 2012.

455 Jaegle, L., Quinn, P. K., Bates, T. S., Alexander, B., and Lin, J. T.: Global distribution of sea salt aerosols: new
456 constraints in situ and remote sensing observations, Atmos. Chem. Phys., 11, 3137-3157,
457 https://doi.org/10.5194/acp-11-3137-2011, 2011.

458 Joshi, R., Liu, D. T., Nemitz, E., Langford, B., Mullinger, N., Squires, F., Lee, J., Wu, Y. F., Pan, X. L., Fu, P.
459 Q., Kotthaus, S., Grimmond, S., Zhang, Q., Wu, R. L., Wild, O., Flynn, M., Coe, H., and Allan, J.: Direct
460 measurements of black carbon fluxes in central Beijing using the eddy covariance method, Atmos. Chem. Phys.,
461 21, 147-162, https://doi.org/10.5194/acp-21-147-2021, 2021.

462 Kondo, Y., Komazaki, Y., Miyazaki, Y., Moteki, N., Takegawa, N., Kodama, D., Deguchi, S., Nogami, M.,
463 Fukuda, M., Miyakawa, T., Morino, Y., Koike, M., Sakurai, H., and Ehara, K.: Temporal variations of elemental
464 carbon in Tokyo, J. Geophys. Res. Atmos., 111, D12205, https://doi.org/10.1029/2005jd006257, 2006.

465 Kong, L., Tang, X., Zhu, J., Wang, Z., Pan, Y., Wu, H., Wu, L., Wu, Q., He, Y., Tian, S., Xie, Y., Liu, Z., Sui,
466 W., Han, L., and Carmichael, G.: Improved Inversion of Monthly Ammonia Emissions in China Based on the
467 Chinese Ammonia Monitoring Network and Ensemble Kalman Filter, Environ. Sci. Technol., 53, 12529-12538,
468 https://doi.org/10.1021/acs.est.9b02701, 2019.

469 Le, T., Wang, Y., Liu, L., Yang, J., Yung, Y. L., Li, G., and Seinfeld, J. H.: Unexpected air pollution with marked
470 emission reductions during the COVID-19 outbreak in China, Science, 369, 702-706,
471 https://doi.org/10.1126/science.abb7431, 2020.

472 Li, C., Li, Q., Tong, D., Wang, Q., Wu, M., Sun, B., Su, G., and Tan, L.: Environmental impact and health risk
473 assessment of volatile organic compound emissions during different seasons in Beijing, J. Environ. Sci. (China),
474 93, 1-12, https://doi.org/10.1016/j.jes.2019.11.006, 2020a.

475 Li, J., Liao, H., Hu, J., and Li, N.: Severe particulate pollution days in China during 2013-2018 and the associated
476 typical weather patterns in Beijing-Tianjin-Hebei and the Yangtze River Delta regions, Environ. Pollut., 248, 74-
477 81, https://doi.org/10.1016/j.envpol.2019.01.124, 2019a.

478 Li, K., Jacob, D. J., Liao, H., Shen, L., Zhang, Q., and Bates, K. H.: Anthropogenic drivers of 2013-2017 trends
479 in summer surface ozone in China, Proc. Natl. Acad. Sci. USA, 116, 422-427,
480 https://doi.org/10.1073/pnas.1812168116, 2019b.

481 Li, K., Liao, H., Mao, Y. H., and Ridley, D. A.: Source sector and region contributions to concentration and direct
482 radiative forcing of black carbon in China, Atmos. Environ., 124, 351-366,
483 https://doi.org/10.1016/j.atmosenv.2015.06.014, 2016.

484 Li, M., Liu, H., Geng, G. N., Hong, C. P., Liu, F., Song, Y., Tong, D., Zheng, B., Cui, H. Y., Man, H. Y., Zhang,
485 Q., and He, K. B.: Anthropogenic emission inventories in China: a review, Natl. Sci. Rev., 4, 834-866,
486 https://doi.org/10.1093/nsr/nwx150, 2017.

487 Li, M., Zhang, Q., Streets, D. G., He, K. B., Cheng, Y. F., Emmons, L. K., Huo, H., Kang, S. C., Lu, Z., Shao, M.,
488 Su, H., Yu, X., and Zhang, Y.: Mapping Asian anthropogenic emissions of non-methane volatile organic
489 compounds to multiple chemical mechanisms, Atmos. Chem. Phys., 14, 5617-5638, https://doi.org/10.5194/acp-
490 14-5617-2014, 2014.

491 Li, M., Zhang, Q., Zheng, B., Tong, D., Lei, Y., Liu, F., Hong, C. P., Kang, S. C., Yan, L., Zhang, Y. X., Bo, Y.,
492 Su, H., Cheng, Y. F., and He, K. B.: Persistent growth of anthropogenic non-methane volatile organic compound
493 (NMVOC) emissions in China during 1990-2017: drivers, speciation and ozone formation potential, Atmos. Chem.
494 Phys., 19, 8897-8913, https://doi.org/10.5194/acp-19-8897-2019, 2019c.

495 Li, Q., Su, G., Li, C., Liu, P., Zhao, X., Zhang, C., Sun, X., Mu, Y., Wu, M., Wang, Q., and Sun, B.: An
496 investigation into the role of VOCs in SOA and ozone production in Beijing, China, Sci. Total. Environ., 720,
497 137536, https://doi.org/10.1016/j.scitotenv.2020.137536, 2020b.

498 Li, X. R., Zhang, C. L., Liu, P. F., Liu, J. F., Zhang, Y. Y., Liu, C. T., and Mu, Y. J.: Significant influence of the
499 intensive agricultural activities on atmospheric $PM_{2.5}$ during autumn harvest seasons in a rural area of the North
500 China Plain, Atmos. Environ., 241, 117844, https://doi.org/10.1016/j.atmosenv.2020.117844, 2020c.

501 Liu, H., Jacob, D. J., Bey, I., and Yantosca, R. M.: Constraints from ^{210}Pb and [7]Be on wet deposition and transport
502 in a global three-dimensional chemical tracer model driven by assimilated meteorological fields, J. Geophys. Res.
503 Atmos., 106, 12109-12128, https://doi.org/10.1029/2000jd900839, 2001.

504 Liu, H., Liu, S., Xue, B. R., Lv, Z. F., Meng, Z. H., Yang, X. F., Xue, T., Yu, Q., and He, K. B.: Ground-level
505 ozone pollution and its health impacts in China, Atmos. Environ., 173, 223-230,
506 https://doi.org/10.1016/j.atmosenv.2017.11.014, 2018a.

507 Liu, M. X., Huang, X., Song, Y., Xu, T. T., Wang, S. X., Wu, Z. J., Hu, M., Zhang, L., Zhang, Q., Pan, Y. P., Liu,
508 X. J., and Zhu, T.: Rapid SO_2 emission reductions significantly increase tropospheric ammonia concentrations
509 over the North China Plain, Atmos. Chem. Phys., 18, 17933-17943, https://doi.org/10.5194/acp-18-17933-2018,
510 2018b.

511 Luo, G., Yu, F. Q., and Moch, J. M.: Further improvement of wet process treatments in GEOS-Chem v12.6.0:
512 impact on global distributions of aerosols and aerosol precursors, Geosci. Model Dev., 13, 2879-2903,
513 https://doi.org/10.5194/gmd-13-2879-2020, 2020.

514 Luo, G., Yu, F. Q., and Schwab, J.: Revised treatment of wet scavenging processes dramatically improves GEOS-
515 Chem 12.0.0 simulations of surface nitric acid, nitrate, and ammonium over the United States, Geosci. Model
516 Dev., 12, 3439-3447, https://doi.org/10.5194/gmd-12-3439-2019, 2019.

517   Ma, Q. A., Cai, S. Y., Wang, S. X., Zhao, B., Martin, R. V., Brauer, M., Cohen, A., Jiang, J. K., Zhou, W., Hao,
518   J. M., Frostad, J., Forouzanfar, M. H., and Burnett, R. T.: Impacts of coal burning on ambient $PM_{2.5}$ pollution in
519   China, Atmos. Chem. Phys., 17, 4477-4491, https://doi.org/10.5194/acp-17-4477-2017, 2017.

520   Martini, F. M. S., Hasenkopf, C. A., and Roberts, D. C.: Statistical analysis of $PM_{2.5}$ observations from diplomatic
521   facilities in China, Atmos. Environ., 110, 174-185, https://doi.org/10.1016/j.atmosenv.2015.03.060, 2015.

522   Ministry of Ecology and Environment, the People's Republic of China (MEE).Ambient air quality standards
523   GB3095-2012   (in   Chinese),   available   at:
524   https://www.mee.gov.cn/ywgz/fgbz/bz/bzwb/dqhjbh/dqhjzlbz/201203/t20120302_224165.shtml (last access: 04
525   March 2021), 2012.

526   Ministry of Ecology and Environment, the People's Republic of China (MEE).Air Pollution Comprehensive
527   Management Action Plan in the Autumn and Winter of 2017-2018 for the Beijing-Tianjin-Hebei Region and its
528   Surrounding   Areas   (in   Chinese),   available   at:
529   https://www.mee.gov.cn/gkml/sthjbgw/sthjbwj/201809/t20180927_630570.htm (last access: 04 March 2021),
530   2017.

531   Ministry of Ecology and Environment, the People's Republic of China (MEE).Letter on notifying the completion
532   of air quality targets in the Beijing-Tianjin-Hebei air pollution transmission channel cities in autumn and winter
533   (in Chinese), available at: http://www.mee.gov.cn/gkml/sthjbgw/stbgth/201805/t20180503_435855.htm (last
534   access: 04 March 2021), 2018.

535   Miao, R. Q., Chen, Q., Zheng, Y., Cheng, X., Sun, Y. L., Palmer, P. I., Shrivastava, M., Guo, J. P., Zhang, Q.,
536   Liu, Y. H., Tan, Z. F., Ma, X. F., Chen, S. Y., Zeng, L. M., Lu, K. D., and Zhang, Y. H.: Model bias in simulating
537   major chemical components of $PM_{2.5}$ in China, Atmos. Chem. Phys., 20, 12265-12284,
538   https://doi.org/10.5194/acp-20-12265-2020, 2020.

539   Moch, J. M., Dovrou, E., Mickley, L. J., Keutsch, F. N., Cheng, Y., Jacob, D. J., Jiang, J. K., Li, M., Munger, J.
540   W., Qiao, X. H., and Zhang, Q.: Contribution of Hydroxymethane Sulfonate to Ambient Particulate Matter: A
541   Potential Explanation for High Particulate Sulfur During Severe Winter Haze in Beijing, Geophys. Res. Lett., 45,
542   11969-11979, https://doi.org/10.1029/2018gl079309, 2018.

543   Pan, Y., Tian, S., Zhao, Y., Zhang, L., Zhu, X., Gao, J., Huang, W., Zhou, Y., Song, Y., Zhang, Q., and Wang,
544   Y.: Identifying Ammonia Hotspots in China Using a National Observation Network, Environ. Sci. Technol., 52,
545   3926-3934, https://doi.org/10.1021/acs.est.7b05235, 2018.

546   Park, R. J., Jacob, D. J., Field, B. D., Yantosca, R. M., and Chin, M.: Natural and transboundary pollution
547   influences on sulfate-nitrate-ammonium aerosols in the United States: Implications for policy, J. Geophys. Res.
548   Atmos., 109, D15204, https://doi.org/10.1029/2003jd004473, 2004.

549   Peng, L. Q., Zhang, Q., Yao, Z. L., Mauzerall, D. L., Kang, S. C., Du, Z. Y., Zheng, Y. X., Xue, T., and He, K.
550   B.: Underreported coal in statistics: A survey-based solid fuel consumption and emission inventory for the rural
551   residential sector in China, Appl. Energ., 235, 1169-1182, https://doi.org/10.1016/j.apenergy.2018.11.043, 2019.

552   Reed, C., Evans, M. J., Di Carlo, P., Lee, J. D., and Carpenter, L. J.: Interferences in photolytic NO2 measurements:
553   explanation for an apparent missing oxidant?, Atmos. Chem. Phys., 16, 4707-4724, https://doi.org/10.5194/acp-
554   16-4707-2016, 2016.

555   Shah, V., Jacob, D. J., Li, K., Silvern, R. F., Zhai, S. X., Liu, M. Y., Lin, J. T., and Zhang, Q.: Effect of changing
556   NO_x lifetime on the seasonality and long-term trends of satellite-observed tropospheric NO_2 columns over China,
557   Atmos. Chem. Phys., 20, 1483-1495, https://doi.org/10.5194/acp-20-1483-2020, 2020.

558 Shi, Y. Q., Xi, Z. Y., Simayi, M., Li, J., and Xie, S. D.: Scattered coal is the largest source of ambient volatile
559 organic compounds during the heating season in Beijing, Atmos. Chem. Phys., 20, 9351-9369,
560 https://doi.org/10.5194/acp-20-9351-2020, 2020.

561 Shi, Z., Song, C., Liu, B., Lu, G., Xu, J., Van Vu, T., Elliott, R. J. R., Li, W., Bloss, W. J., and Harrison, R. M.:
562 Abrupt but smaller than expected changes in surface air quality attributable to COVID-19 lockdowns, Sci. Adv.,
563 7, eabd6696, https://doi.org/10.1126/sciadv.abd6696, 2021.

564 Shi, Z. B., Vu, T., Kotthaus, S., Harrison, R. M., Grimmond, S., Yue, S., Zhu, T., Lee, J., Han, Y., Demuzere, M.,
565 Dunmore, R. E., Ren, L. J., Liu, D., Wang, Y. L., Wild, O., Allan, J., Acton, W. J., Barlow, J., Barratt, B., Beddows,
566 D., Bloss, W. J., Calzolai, G., Carruthers, D., Carslaw, D. C., Chan, Q., Chatzidiakou, L., Chen, Y., Crilley, L.,
567 Coe, H., Dai, T., Doherty, R., Duan, F., Fu, P., Ge, B., Ge, M., Guan, D., Hamilton, J. F., He, K., Heal, M., Heard,
568 D., Hewitt, C. N., Hollaway, M., Hu, M., Ji, D., Jiang, X. J., Jones, R., Kalberer, M., Kelly, F. J., Kramer, L.,
569 Langford, B., Lin, C., Lewis, A. C., Li, J., Li, W., Liu, H., Liu, J. F., Loh, M., Lu, K. D., Lucarelli, F., Mann, G.,
570 McFiggans, G., Miller, M. R., Mills, G., Monk, P., Nemitz, E., O'Connor, F., Ouyang, B., Palmer, P. I., Percival,
571 C., Popoola, O., Reeves, C., Rickard, A. R., Shao, L. Y., Shi, G. Y., Spracklen, D., Stevenson, D., Sun, Y., Sun,
572 Z. W., Tao, S., Tong, S. R., Wang, Q. Q., Wang, W. H., Wang, X. M., Wang, X. J., Wang, Z. F., Wei, L. F.,
573 Whalley, L., Wu, X. F., Wu, Z. J., Xie, P. H., Yang, F. M., Zhang, Q., Zhang, Y. L., Zhang, Y. H., and Zheng,
574 M.: Introduction to the special issue "In-depth study of air pollution sources and processes within Beijing and its
575 surrounding region (APHH-Beijing)", Atmos. Chem. Phys., 19, 7519-7546, https://doi.org/10.5194/acp-19-7519-
576 2019, 2019.

577 Silver, B., Reddington, C. L., Arnold, S. R., and Spracklen, D. V.: Substantial changes in air pollution across
578 China during 2015-2017, Environ. Res. Lett., 13, 114012, https://doi.org/10.1088/1748-9326/aae718, 2018.

579 Song, S. J., Gao, M., Xu, W. Q., Sun, Y. L., Worsnop, D. R., Jayne, J. T., Zhang, Y. Z., Zhu, L., Li, M., Zhou, Z.,
580 Cheng, C. L., Lv, Y. B., Wang, Y., Peng, W., Xu, X. B., Lin, N., Wang, Y. X., Wang, S. X., Munger, J. W., Jacob,
581 D. J., and McElroy, M. B.: Possible heterogeneous chemistry of hydroxymethanesulfonate (HMS) in northern
582 China winter haze, Atmos. Chem. Phys., 19, 1357-1371, https://doi.org/10.5194/acp-19-1357-2019, 2019.

583 Squires, F. A., Nemitz, E., Langford, B., Wild, O., Drysdale, W. S., Acton, W. J. F., Fu, P. Q., Grimmond, C. S.
584 B., Hamilton, J. F., Hewitt, C. N., Hollaway, M., Kotthaus, S., Lee, J., Metzger, S., Pingintha-Durden, N., Shaw,
585 M., Vaughan, A. R., Wang, X. M., Wu, R. L., Zhang, Q., and Zhang, Y. L.: Measurements of traffic-dominated
586 pollutant emissions in a Chinese megacity, Atmos. Chem. Phys., 20, 8737-8761, https://doi.org/10.5194/acp-20-
587 8737-2020, 2020.

588 Taiwo, A. M., Beddows, D. C., Calzolai, G., Harrison, R. M., Lucarelli, F., Nava, S., Shi, Z., Valli, G., and Vecchi,
589 R.: Receptor modelling of airborne particulate matter in the vicinity of a major steelworks site, Sci. Total. Environ.,
590 490, 488-500, https://doi.org/10.1016/j.scitotenv.2014.04.118, 2014.

591 Tong, R. P., Liu, J. F., Wang, W., and Fang, Y. Q.: Health effects of $PM_{2.5}$ emissions from on-road vehicles during
592 weekdays and weekends in Beijing, China, Atmos. Environ., 223, 117258,
593 https://doi.org/10.1016/j.atmosenv.2019.117258, 2020.

594 Vu, T. V., Shi, Z. B., Cheng, J., Zhang, Q., He, K. B., Wang, S. X., and Harrison, R. M.: Assessing the impact of
595 clean air action on air quality trends in Beijing using a machine learning technique, Atmos. Chem. Phys., 19,
596 11303-11314, https://doi.org/10.5194/acp-19-11303-2019, 2019.

597 Wan, Y. T., Xu, M. Y., Huang, H., and Chen, S. X.: A spatio-temporal model for the analysis and prediction of
598 fine particulate matter concentration in Beijing, Environmetrics, 32, e2648, https://doi.org/10.1002/env.2648,
599 2021.

600 Wang, G., Zhang, R., Gomez, M. E., Yang, L., Levy Zamora, M., Hu, M., Lin, Y., Peng, J., Guo, S., Meng, J., Li,
601 J., Cheng, C., Hu, T., Ren, Y., Wang, Y., Gao, J., Cao, J., An, Z., Zhou, W., Li, G., Wang, J., Tian, P., Marrero-
602 Ortiz, W., Secrest, J., Du, Z., Zheng, J., Shang, D., Zeng, L., Shao, M., Wang, W., Huang, Y., Wang, Y., Zhu, Y.,

603   Li, Y., Hu, J., Pan, B., Cai, L., Cheng, Y., Ji, Y., Zhang, F., Rosenfeld, D., Liss, P. S., Duce, R. A., Kolb, C. E.,
604   and Molina, M. J.: Persistent sulfate formation from London Fog to Chinese haze, Proc. Natl. Acad. Sci. USA,
605   113, 13630-13635, https://doi.org/10.1073/pnas.1616540113, 2016.

606   Wang, J., Li, J., Ye, J., Zhao, J., Wu, Y., Hu, J., Liu, D., Nie, D., Shen, F., Huang, X., Huang, D. D., Ji, D., Sun,
607   X., Xu, W., Guo, J., Song, S., Qin, Y., Liu, P., Turner, J. R., Lee, H. C., Hwang, S., Liao, H., Martin, S. T., Zhang,
608   Q., Chen, M., Sun, Y., Ge, X., and Jacob, D. J.: Fast sulfate formation from oxidation of SO_2 by NO_2 and HONO
609   observed in Beijing haze, Nat. Commun., 11, 2844, https://doi.org/10.1038/s41467-020-16683-x, 2020.

610   Wang, J., Ye, J., Zhang, Q., Zhao, J., Wu, Y., Li, J., Liu, D., Li, W., Zhang, Y., Wu, C., Xie, C., Qin, Y., Lei, Y.,
611   Huang, X., Guo, J., Liu, P., Fu, P., Li, Y., Lee, H. C., Choi, H., Zhang, J., Liao, H., Chen, M., Sun, Y., Ge, X.,
612   Martin, S. T., and Jacob, D. J.: Aqueous production of secondary organic aerosol from fossil-fuel emissions in
613   winter Beijing haze, Proc. Natl. Acad. Sci. USA, 118, e2022179118, https://doi.org/10.1073/pnas.2022179118,
614   2021.

615   Wang, Y., Jacob, D. J., and Logan, J. A.: Global simulation of tropospheric O_3-NO_x-hydrocarbon chemistry: 1.
616   Model formulation, J. Geophys. Res. Atmos., 103, 10713-10725, https://doi.org/10.1029/98jd00158, 1998.

617   Wang, Y., Ying, Q., Hu, J., and Zhang, H.: Spatial and temporal variations of six criteria air pollutants in 31
618   provincial capital cities in China during 2013-2014, Environ. Int., 73, 413-422,
619   https://doi.org/10.1016/j.envint.2014.08.016, 2014.

620   Wang, Y., Zhang, Q. Q., He, K., Zhang, Q., and Chai, L.: Sulfate-nitrate-ammonium aerosols over China: response
621   to 2000-2015 emission changes of sulfur dioxide, nitrogen oxides, and ammonia, Atmos. Chem. Phys., 13, 2635-
622   2652, https://doi.org/10.5194/acp-13-2635-2013, 2013.

623   Wang, Y. S., Li, W. J., Gao, W. K., Liu, Z. R., Tian, S. L., Shen, R. R., Ji, D. S., Wang, S., Wang, L. L., Tang, G.
624   Q., Song, T., Cheng, M. T., Wang, G. H., Gong, Z. Y., Hao, J. M., and Zhang, Y. H.: Trends in particulate matter
625   and its chemical compositions in China from 2013-2017, Sci. China Earth Sci., 62, 1857-1871,
626   https://doi.org/10.1007/s11430-018-9373-1, 2019.

627   Wu, H. J., Tang, X., Wang, Z. F., Wu, L., Lu, M. M., Wei, L. F., and Zhu, J.: Probabilistic Automatic Outlier
628   Detection for Surface Air Quality Measurements from the China National Environmental Monitoring Network,
629   Adv. Atmos. Sci., 35, 1522-1532, https://doi.org/10.1007/s00376-018-8067-9, 2018.

630   Wu, J., Bei, N., Hu, B., Liu, S., Zhou, M., Wang, Q., Li, X., Liu, L., Feng, T., Liu, Z., Wang, Y., Cao, J., Tie, X.,
631   Wang, J., Molina, L. T., and Li, G.: Is water vapor a key player of the wintertime haze in North China Plain?,
632   Atmos. Chem. Phys., 19, 8721-8739, https://doi.org/10.5194/acp-19-8721-2019, 2019.

633   Xie, L. Y., Huang, Y., and Qin, P.: Spatial distribution of coal-fired power plants in China, Environ. Dev. Econ.,
634   23, 495-515, https://doi.org/10.1017/S1355770x18000098, 2018.

635   Xing, L., Fu, T. M., Cao, J. J., Lee, S. C., Wang, G. H., Ho, K. F., Cheng, M. C., You, C. F., and Wang, T. J.:
636   Seasonal and spatial variability of the OM/OC mass ratios and high regional correlation between oxalic acid and
637   zinc in Chinese urban organic aerosols, Atmos. Chem. Phys., 13, 4307-4318, https://doi.org/10.5194/acp-13-
638   4307-2013, 2013.

639   Xu, J., Liu, D., Wu, X., Vu, T. V., Zhang, Y., Fu, P., Sun, Y., Xu, W., Zheng, B., Harrison, R. M., and Shi, Z.:
640   Source apportionment of fine organic carbon at an urban site of Beijing using a chemical mass balance model,
641   Atmos. Chem. Phys., 21, 7321-7341, https://doi.org/10.5194/acp-21-7321-2021, 2021.

642   Yang, G., Liu, Y., and Li, X.: Spatiotemporal distribution of ground-level ozone in China at a city level, Sci. Rep.,
643   10, 7229, https://doi.org/10.1038/s41598-020-64111-3, 2020.

644 Yun, X., Shen, G., Shen, H., Meng, W., Chen, Y., Xu, H., Ren, Y., Zhong, Q., Du, W., Ma, J., Cheng, H., Wang,
645 X., Liu, J., Wang, X., Li, B., Hu, J., Wan, Y., and Tao, S.: Residential solid fuel emissions contribute significantly
646 to air pollution and associated health impacts in China, Sci. Adv., 6, eaba7621,
647 https://doi.org/10.1126/sciadv.aba7621, 2020.

648 Zhai, S. X., Jacob, D. J., Wang, X., Shen, L., Li, K., Zhang, Y. Z., Gui, K., Zhao, T. L., and Liao, H.: Fine
649 particulate matter (PM$_{2.5}$) trends in China, 2013-2018: separating contributions from anthropogenic emissions and
650 meteorology, Atmos. Chem. Phys., 19, 11031-11041, https://doi.org/10.5194/acp-19-11031-2019, 2019.

651 Zhang, F., Shi, Y., Fang, D., Ma, G., Nie, C., Krafft, T., He, L., and Wang, Y.: Monitoring history and change
652 trends of ambient air quality in China during the past four decades, J. Environ. Manage, 260, 110031,
653 https://doi.org/10.1016/j.jenvman.2019.110031, 2020.

654 Zhang, Q., Zheng, Y., Tong, D., Shao, M., Wang, S., Zhang, Y., Xu, X., Wang, J., He, H., Liu, W., Ding, Y., Lei,
655 Y., Li, J., Wang, Z., Zhang, X., Wang, Y., Cheng, J., Liu, Y., Shi, Q., Yan, L., Geng, G., Hong, C., Li, M., Liu,
656 F., Zheng, B., Cao, J., Ding, A., Gao, J., Fu, Q., Huo, J., Liu, B., Liu, Z., Yang, F., He, K., and Hao, J.: Drivers of
657 improved PM$_{2.5}$ air quality in China from 2013 to 2017, Proc. Natl. Acad. Sci. USA, 116, 24463-24469,
658 https://doi.org/10.1073/pnas.1907956116, 2019.

659 Zhang, X., Wu, Y., Liu, X., Reis, S., Jin, J., Dragosits, U., Van Damme, M., Clarisse, L., Whitburn, S., Coheur,
660 P. F., and Gu, B.: Ammonia Emissions May Be Substantially Underestimated in China, Environ. Sci. Technol.,
661 51, 12089-12096, https://doi.org/10.1021/acs.est.7b02171, 2017a.

662 Zhang, Y., Cai, J., Wang, S., He, K., and Zheng, M.: Review of receptor-based source apportionment research of
663 fine particulate matter and its challenges in China, Sci. Total. Environ., 586, 917-929,
664 https://doi.org/10.1016/j.scitotenv.2017.02.071, 2017b.

665 Zhang, Y., Chen, X., Yu, S., Wang, L., Li, Z., Li, M., Liu, W., Li, P., Rosenfeld, D., and Seinfeld, J. H.: City-
666 level air quality improvement in the Beijing-Tianjin-Hebei region from 2016/17 to 2017/18 heating seasons:
667 Attributions and process analysis, Environ. Pollut., 274, 116523, https://doi.org/10.1016/j.envpol.2021.116523,
668 2021.

669 Zhang, Y. P., Li, X., Nie, T., Qi, J., Chen, J., and Wu, Q.: Source apportionment of PM$_{2.5}$ pollution in the central
670 six districts of Beijing, China, J. Clean Prod., 174, 661-669, https://doi.org/10.1016/j.jclepro.2017.10.332, 2018.

671 Zheng, B., Tong, D., Li, M., Liu, F., Hong, C. P., Geng, G. N., Li, H. Y., Li, X., Peng, L. Q., Qi, J., Yan, L.,
672 Zhang, Y. X., Zhao, H. Y., Zheng, Y. X., He, K. B., and Zhang, Q.: Trends in China's anthropogenic emissions
673 since 2010 as the consequence of clean air actions, Atmos. Chem. Phys., 18, 14095-14111,
674 https://doi.org/10.5194/acp-18-14095-2018, 2018.

675 Zheng, M., Yan, C. Q., Wang, S. X., He, K. B., and Zhang, Y. H.: Understanding PM$_{2.5}$ sources in China:
676 challenges and perspectives, Natl. Sci. Rev., 4, 801-803, https://doi.org/10.1093/nsr/nwx129, 2017.
677

678

679
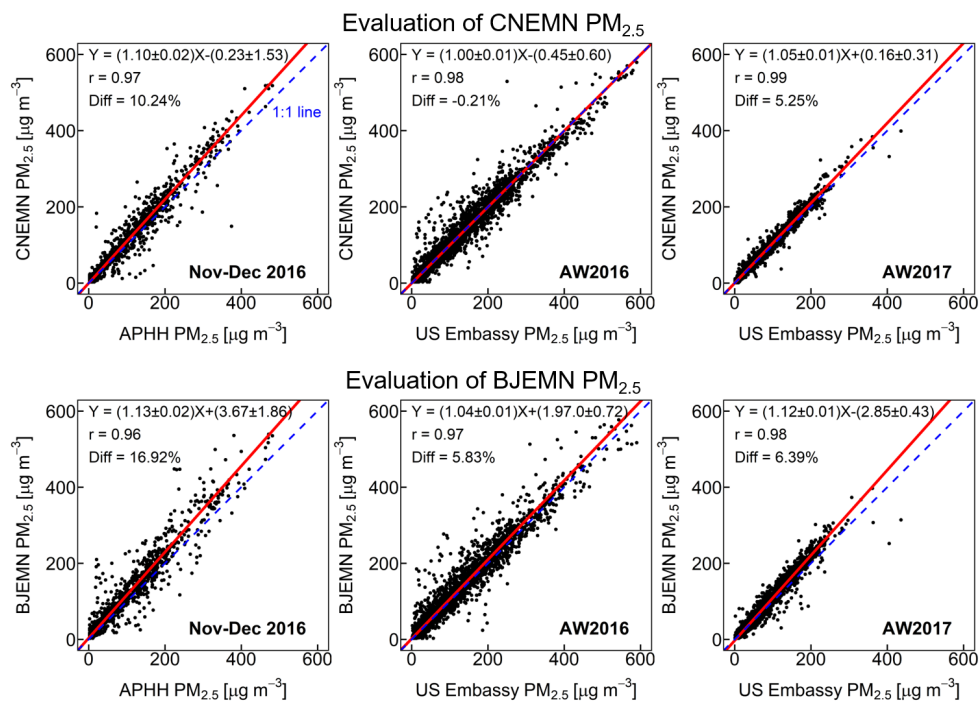
680

681 **Figure 1.** Evaluation of local and national network PM$_{2.5}$ measurements. Points are hourly PM$_{2.5}$ measurements. The top row
682 compares CNEMN to the APHH urban site (left), and CNEMN to the US Embassy in autumn-winter 2016/2017 (AW2016)
683 (centre) and 2017/2018 (AW2017) (right). The bottom row compares BJMEMN to the APHH urban site (left), and BJMEMN
684 to the US Embassy in AW2016 (centre) and AW2017 (right). Reduced major axis (RMA) regression statistics, Pearson's
685 correlation coefficients (r), and the percent difference (Diff = monitoring network minus independent measurement) are given.
686 Lines are the RMA regression (red) and 1:1 line (blue dashed).

687

688
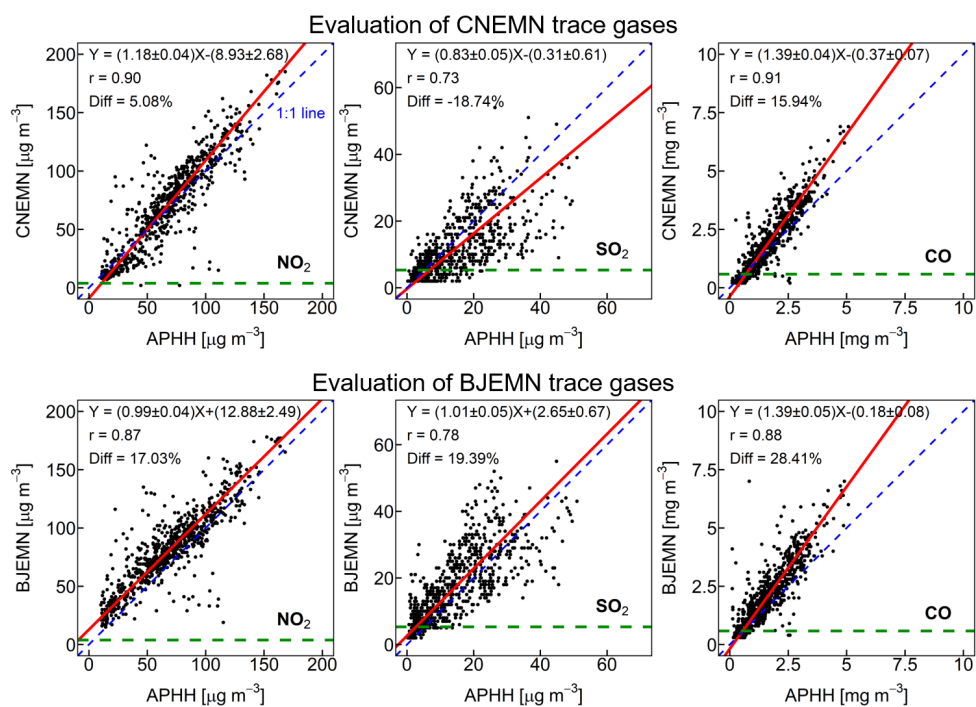
Figure 2. Evaluation of local and national network trace gas concentration measurements. Points are hourly measurements.
Panels compare CNEMN (top) and BJMEMN (bottom) NO_2 (left), SO_2 (centre) and CO (right) to the APHH urban site in
November-December 2016. RMA regression statistics, Pearson's correlation coefficients (r), and the percent difference (Diff
= monitoring network minus independent measurement) are given. Lines are the RMA regression (red) and 1:1 line (blue
dashed). The green dashed line is the reported monitoring network instrument detection limit (MEE, 2012).

694
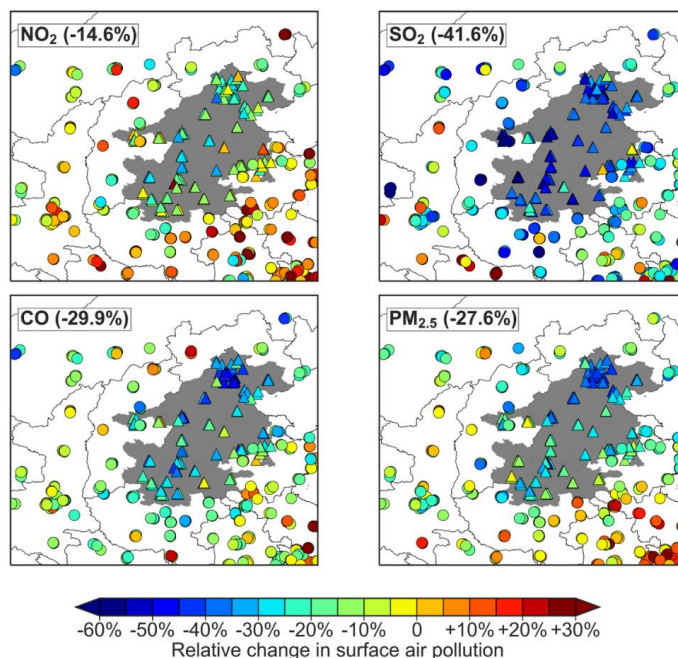
Figure 3. Change in surface air pollution in BTH and the surrounding area in AW2017 relative to AW2016. Individual points are monitoring network site changes for the target region (triangles within area shaded grey) and the surrounding area (circles in the non-shaded area). Values inset give the percent change for sites in the grey domain only. Note the colourbar is uneven.

700

701
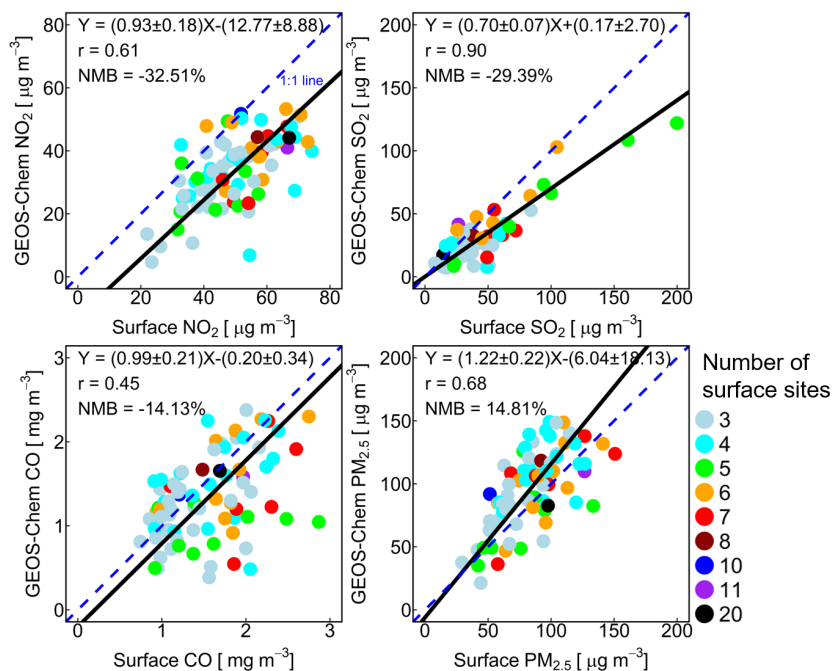
Figure 4. Evaluation of GEOS-Chem simulation of air pollutant concentrations in AW2016. Observations are averaged onto the GEOS-Chem grid. Points are simulated and observed NO_2 (top left), SO_2 (top right), CO (bottom left) and $PM_{2.5}$ (bottom right) in the entire domain in Figure 3 for grid squares with at least three coincident surface sites. Points are coloured by the number of surface sites. The model uses scaled MEIC emissions (see text for details). RMA regression statistics, Pearson's correlation coefficients (r), and model normalized mean biases (NMB) are given. Lines are the RMA regression (black) and 1:1 line (blue dashed).

708
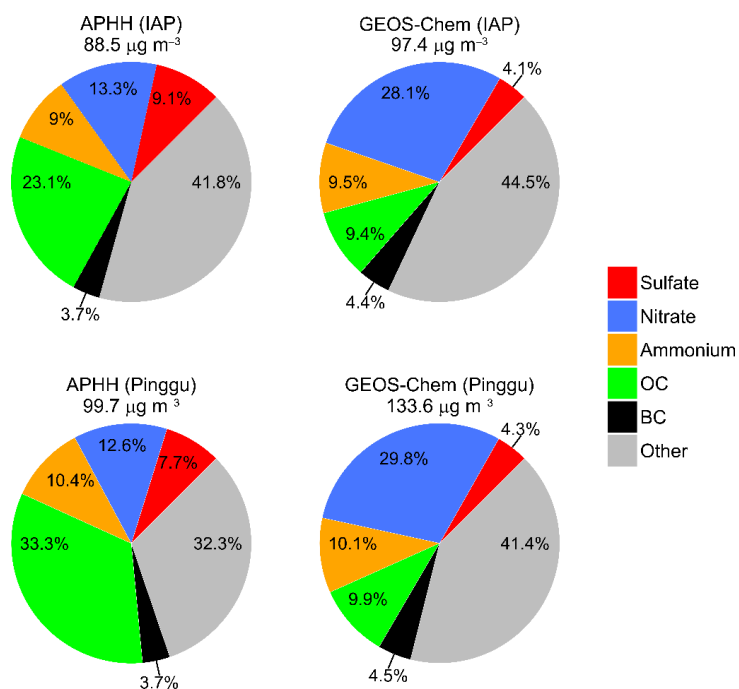
Figure 5. Relative contribution of individual PM$_{2.5}$ components during the APHH campaign. Panels are measured (left) and modelled (right) percent contribution for the urban IAP (top) and rural Pinggu (bottom) sites. Components are sulfate, nitrate, ammonium, OC, BC and Other. Other is the sum of trace metals, mineral dust and other ions, the non-carbon portion of OC, and aerosol water at 33-35% relative humidity (RH) for the measurements and 35% RH for the model. Values above the pies are mean total PM$_{2.5}$.

716

717
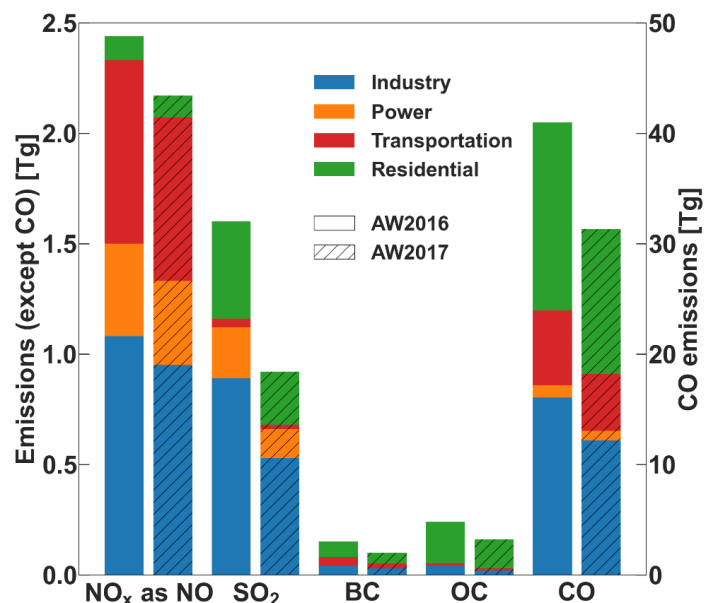
Figure 6. Total anthropogenic emissions in BTH in AW2016 and AW2017. Emissions are for grids covering the grey shaded area in Figure 3. Emissions are from the MEIC with scaling factors to address discrepancies between the model and observations for AW2016 and to reproduce the change in air pollutant concentrations in the AW2017 emission control period (see text for details). Vertical axes are emissions for NO, BC, OC, and SO_2 on the left axis and for CO on the right axis.

722

723

724

725

726

727
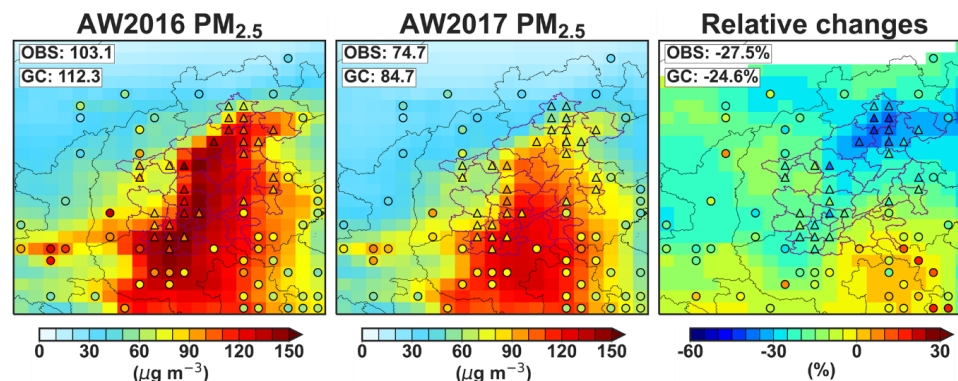
Figure 7. Spatial distribution of absolute and relative changes in observed and modelled $PM_{2.5}$ before and during the strict emission control period. The observed (shapes) and modelled (background) $PM_{2.5}$ are shown for AW2016 (left) and AW2017 (centre). The right panel is the relative change in observed and modelled $PM_{2.5}$. Observations are distinguished as within (triangles) and outside (circles) the emission control region (grey area in Figure 3). Inset values are the observed (OBS) and modelled (GC) means for sites and coincident grids in the emission control domain. Note the uneven colour scale in the right panel.

734
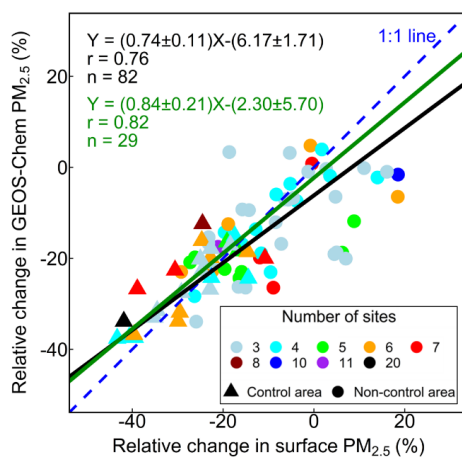
Figure 8. Comparison of observed and modelled relative changes in $PM_{2.5}$. Triangles indicate data in BTH (grey area in Figure 3) and circles indicate data outside BTH. These are coloured by the number of sites in each GEOS-Chem grid. The RMA regression statistics and lines, Pearson's correlation coefficients (r), and NMB are given for all points (black text) and for those in BTH (green text).

739